SAND2018-4642J

Phase-locked photonic wire lasers by conjugation

Ali Khalatpour[1], John L. Reno[2], and Qing Hu[1]

[1]Department of Electrical Engineering and Computer Science and Research Laboratory of Electronics, Massachusetts Institute of Technology, Cambridge, MA 02139, USA

[2]Sandia National Laboratories, Center of Integrated Nanotechnologies, Albuquerque, NM 87185-130, USA

Sandia National Laboratories is a multimission laboratory managed and operated by National Technology & Engineering Solutions of Sandia, LLC, a wholly owned subsidiary of Honeywell International Inc., for the U.S. Department of Energy's National Nuclear Security Administration under contract DE-NA0003525.

Abstract

The term photonic wire laser is now widely used for lasers with transverse dimensions much smaller than the wavelength. As a result, a large fraction of mode propagates outside of the solid core. Here we propose and demonstrate a scheme to form a coupled cavity by taking advantage of this unique feature of photonic wire lasers. In this scheme, we used quantum cascade lasers with antenna-coupled third-order distributed feedback grating (ADFB) as the platform. Inspired by chemistry of hybridization, our scheme phase locks two such lasers by conjugation. With such a coupled-cavity laser, we have demonstrated several performance metrics that are important for various applications in sensing and imaging: 1) a continuous electrical tuning of ~10 GHz at ~ 3.8 THz (fractional tuning of ~0.26%) 2) a good level of output power and power efficiency (~50 mW of continuous-wave power and 0.75% power efficiency), and 3) tight beam patterns (~15^0 of beam divergence).

Introduction

In a photonic wire laser[1-5], which are characterized as $w << \lambda$ (where w is the dimension of the cross section and λ is the wavelength), a large fraction of the mode propagates outside of the deep subwavelength core. This unique feature was utilized in a tunable laser whose frequency can be changed by moving an object placed alongside of the wire laser[6]. Achieving tight beam pattern, single frequency, and high output power in such lasers is a challenging task due to the deep subwavelength transverse dimensions. Moreover, in many applications, electrically tuning of the laser frequency is crucial, in addition to high output power and tight beam patterns. For example, recent development in QCL technology has enabled NASA to initiate the Galactic/Extragalactic ULDB Spectroscopic Terahertz Observatory (GUSTO)[7] that

will measure emissions from the interstellar medium. Measurement of neutral oxygen line (OI at 4.744 THz), which will provide important information on star formation, is at the heart of this mission[8-9]. The highest linear velocity of the interstellar medium in Milky Way[10] is ~250 km/s which will yield a Doppler shift ±0.08%, corresponding to ±4 GHz at 4.744 THz. Hence, a local oscillator which can be electrically tuned over ~8 GHz will be essential for the mapping of the OI line over the entire Milky Way. Besides the specific spectral line in GUSTO, the frequency range of 1-5 THz is also rich with spectral fingerprints of many biochemical species. For instance, low-frequency vibrations of biotin (I) was investigated in the range of 0.8-3.8 THz to better understand the conformational flexibility responsible for its bioactivity[11]. Applications in breast cancer imaging[12], skin cancer imaging[13], colon cancer imaging[14], brain imaging[15-16], identifying explosives[17], checking for defects in airplanes[18], and identifying protein structures[19] have been demonstrated in the same frequency range. THz imaging system based on a double heterodyne detection scheme[20] has yielded a signal/noise ratio of 110 dB. Such a large S/N ratio and the corresponding dynamic range will be very useful in enhancing the imaging capability. In this scheme, the required output power is ~ 50 mW in cw operations which is not easily accessible and was previously done by using bulky far-infrared gas lasers. Therefore, achieving >8 GHz of electrical frequency tuning and CW output power > 50 mW and high beam quality would be of great interest in various applications.

Significant attempt has been made to improve wire laser performance in THz range in terms of output power and power efficiency, beam patterns, and frequency tunability. Recently, up to 1% wall plug efficiency with ~16 mW of CW power and single frequency operation by using a unidirectional antenna coupled third order DFB has been demonstrated[21]. However, no frequency tuning is demonstrated from those devices. In another work, by using piezoelectric

actuators and an intra-cryostat cavity, tuning of ~260 GHz at a center frequency of 3.3 THz is demonstrated with ~5 mW CW power[22-23]. Frequency tuning of a terahertz quantum cascade wire laser over a broad range of ~330 GHz is demonsrated with a moveable MEMS (microelectromechanical systems) side object (plunger) actuated by force[24]and electrical bias[25] to manipulate the transverse optical mode. For pure electrical tuning, it has been demonstrated[26] that a laser device based on a coupled cavity, in which two "knobs" can be tuned by independently biasing the two cavities, can achieve electrical tuning with a good range ~4 GHz (within 50% of output power variation) and 0.7 mW of maximum CW power.

Our scheme to achieve high-power tunable lasers is based on phase locking of two wire lasers so that together they form a coupled cavity. A robust phase locking requires a strong coupling among the individual lasers so that otherwise-independent oscillators are forced to oscillate in sync. Thus far, there are five major demonstrated coupling schemes to phase-lock integrated diode laser arrays. Laser ridges can be coupled through exponentially decaying fields outside the high refractive-index dielectric core[27] (evanescent-wave coupled), or through the Talbot feedback from external reflectors[28-29] (Diffraction-wave coupled), or by connecting two ridges to one single-mode waveguide[30-31] (Y-coupled), or through lateral propagating waves[32-34] (Leaky-wave coupled), or through mutual antenna coupling in far field[35]. The evanescent-wave coupled scheme could be possibly used for two wire lasers with ridge waveguides. However, ridge waveguides have very divergent beam pattern and low extraction efficiency. Diffraction wave coupling can also be used for wire lasers by introducing suitable external feedback components. However, this scheme requires an external component and delicate alignment. The scheme of Y coupled ridge waveguides does not work well with DFB lasers, as the strong reflection in a DFB structure limits its facet coupling. Leaky-wave coupled schemes are not

applicable to DFB structures as the radiation is mostly from radiation apertures and not the facets. Global antenna coupling has been demonstrated recently[35] for phase locking and the mechanism is applicable to wire lasers. However, it is unclear if the phase locking can still be maintained if individual elements are pumped at different currents, which is a neccessity for frequency tuning.

Here, we present a new scheme for phase locking of two wire lasers to form a coupled cavity. We chose quantum cascade lasers (QCL) with antenna coupled third order distributed feedback grating (ADFB) as our platform[36]. ADFBs are a superior platform because of their tight beam pattern, high radiation loss, and high wall plug efficiency (output optical power/input electrical power). Single-mode operation, high CW output power ~ 16 mW, 1% wall plug efficiency (WPE) and tight beam patterns have been already demonstrated in this platform[21]. Schematic of an ADFB is shown in Figure 1.a. When a perfect phase-matching condition is met, the modal index $n_{eff} = \frac{3\lambda_0}{2\,\Lambda} = 3$, the radiations from all the antenna loops are in phase along the DFB structure, resulting in a tight far-field beam pattern[36]. Antenna loop increases the radiation ("mirror") loss by increasing the effective surface area for the radiation aperture. At resonance, the phases of the electric field inside the gaps are the same on both sides of the gap, thus the antenna length L should be equal to $m * \lambda_G$ where m is a positive integer and λ_G is the wavelength in the antenna loop.

One can see in ADFB, the radiation is mostly from the antenna loop. Due to negligible facet radiation, Y and diffraction grating coupling schemes are not applicable here. Since the antenna loop length is determined by resonance condition, ADFB pairs are ~λ_G (defined above) apart and the evanescent lateral coupling is negligible. Since an ADFB even with only a few periods produces a tight beam pattern, far field coupling through mutual antenna coupling is also

not applicable here as this scheme relies on a very divergent beam pattern from individual lasers. Simulation suggests that the fundamental DFB mode is largely confined longitudinally near the center portion of the array. This mode confinement and negligible radiation from facets limits the leaky wave coupling using 180^0 bent cavities at the rear or front facets.[34]

Through this discussion, one can infer that the phase locking of two ADFBs requires a new coupling mechanism, which is the π-coupling reported in this work. As a photonic wire laser, the radiation from each subwavelength aperture is very divergent. A simulated radiation profile of a single-period third order DFB with (ADFB) and without antenna loop is shown in 1.b. It can be observed that by attaching the antenna loop, not only the mirror loss increases, but also the lateral radiation in intermediate zone ($\sim\lambda$) is significantly enhanced. The strong lateral field distribution opens up the possibility for π-coupling of two or even more ADFBs. Since the coupling exists between all in-phase antenna loops, this scheme will be far more effective compared to earlier schemes. Same cannot be said for a third order grating without the antenna loop. Even though the beam from the radiating aperture is divergent, there is no strong coupling to an adjacent gap through π coupling.

Since strong coupling will reduce the mirror loss α_m for the coupled cavities[35], it can be used to quantify the coupling strength. As shown in 1.c, α_m for the third order DFB without the antenna loop[37] is only reduced marginally (~8%) as they are brought close to each other, indicating a negligible π coupling between the two. In addition to that, for very closely spaced cavities, the asymmetric mode has a lower radiation loss and it will be the lasing mode as it has a quadrupole moment with a lower radiation loss than dipole moment. On the other hand, as shown in Fig. 1.d, α_m for ADFBs is significantly reduced as they are brought closer to each other due to strong π coupling of the in-phase aperture fields. We further notice that the cavities are

decoupled for distance more than a few wavelengths suggesting that the coupling mechanism is not strong in the far field. Even at the closest distance between the antenna loops, the center to center radiating apertures are ~λ_G apart so evanescent wave coupling is negligible, but α_m is reduced by ~50% indicating a strong coupling. However, even though evanescent coupling does not have much impact on the π coupling mechanism, it greatly impacts mode selectivity between symmetric and asymmetric supermode in our scheme. As mentioned earlier, the first order antenna loop length is λ_G in which λ_G is the wavelength in the antenna loop. If we we neglect the gap between the loops, the distance between the two parallel radiation appertures is ~$2\times\frac{\lambda_G}{2}$. Since there is strong local coupling between two ADFBs through evanescence waves at the gap between the two antenna loops, the resonance condition of ADFBs favors the symmetric supermode (in phase, ~λ_G apart) over the asymmetric supermode.

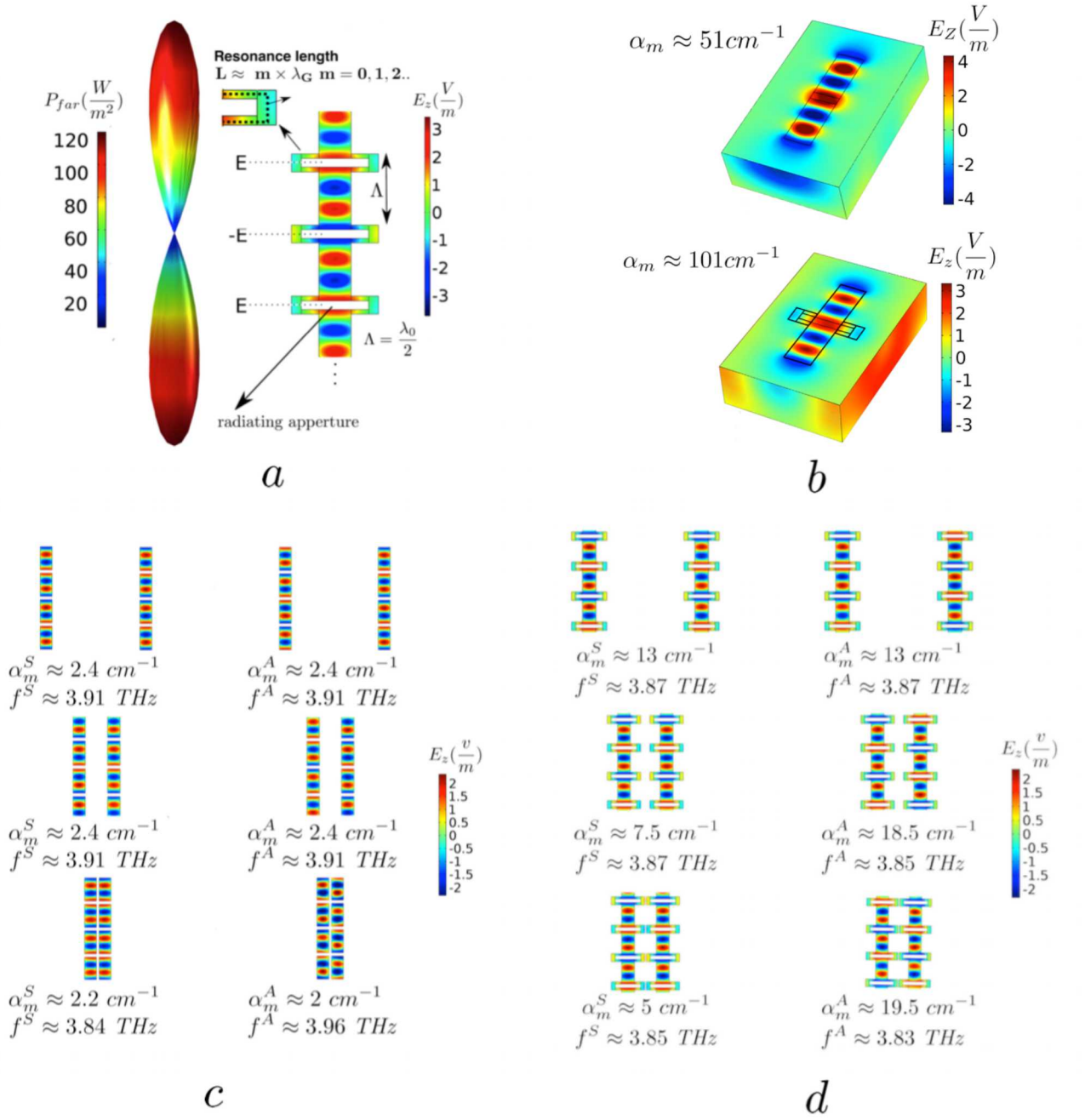

Figure 1. a. Schematic of simulated fundamental mode and the beam pattern of an ADFB, b. Comparison between lateral intermediate zone radiation of a short (with two periods) third order DFB with and without antenna loop, **c**. mirror loss α_m for a supermode formed in π-coupled DFB (without the loop antenna) with center-to-center distance of $\approx 2\lambda_0, \frac{3\lambda_0}{4}, \frac{\lambda_0}{4}$. Superscripts S is for symmetric supermode and superscripts A is for assymetric suppermode. **d**. α_m for a supermode formed in π-coupled ADFB with center to center distance of $\approx 2\lambda_0, \frac{3\lambda_0}{4}, \frac{\lambda_0}{2}$.

Results and discussion

To implement the idea, we fabricated an array of π-coupled ADFBs. A schematic of the array along with other fabrication geometry details are shown in Figure 2. Each array has 10 pairs of π-coupled ADFB. The antenna loop length is varied from one pair to another to adjust the resonance condition. The distance between the pairs are designed to be sufficiently large to avoid inter-pair coupling. Considering the fabrication resolution, the gap between the antenna loops is set to be $\frac{\lambda_0}{40}$ =2μm. The size of the gap within the antenna loop is 5.5 μm to ensure high mirror loss α_m for the super mode. Based on the simulations, α_m for the super mode is 40% of an uncoupled one and predicted to be 6 cm^{-1} for the symmetric supermode in π-coupled ADFB. The center frequency of π-coupled ADFB in this chip is designed to be around 3 GHz apart from the adjacent pair (by simply increasing the antenna loop length by 4%, monotonically decreasing frequency shift can be achieved).

The measurement results are shown in Figure 2.e and 2.f. The observed inter dependence of current thresholds and single lobe beam pattern is a strong evidence for a symmetric supermode. In perticular, no lasing was observed if one ADFB was unbiased suggetsing a significant loss in the cold cavity and a strong coupling between the two. When both are biased, as the bias for one ADFB increased, the lasing treshold for the bias of the other ADFB decreased indicating the total gain increased in the coupled cavity.

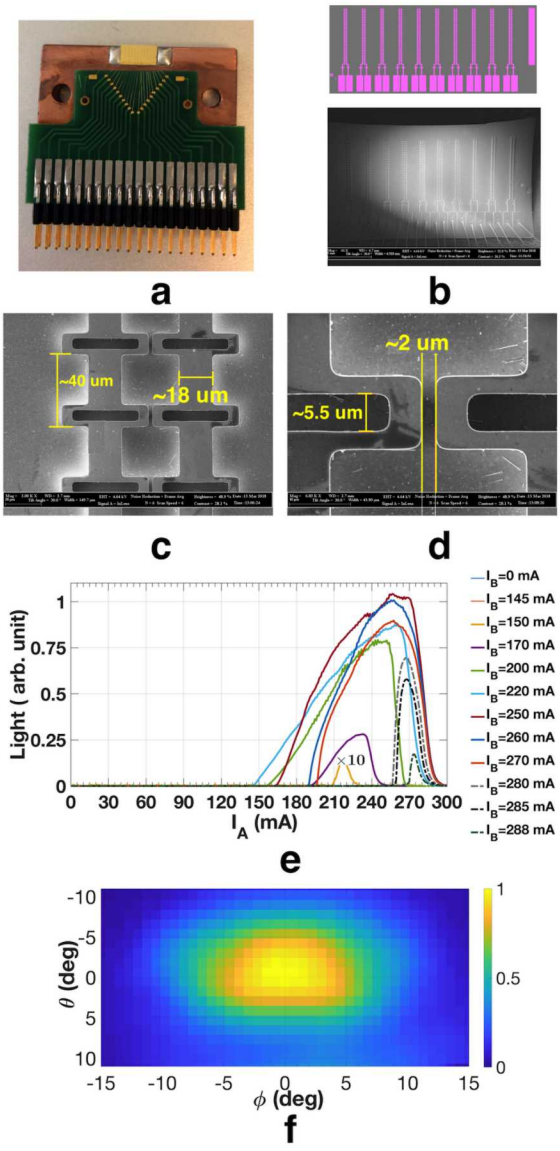

Figure 2: **a**. Eectronic chip for simultaneous independent biasing, **b**. A fabricated die with 10 pairs of π-coupled ADFBs, **c**. Three periods shown (from total 35 periods) in the fabricated π-coupled ADFB, **d**. Magnified SEM image of the air gap between the antenna loops, **e**. light-current curves, **f**. beam pattern

To measure a possible frequency offset between π-coupled ADFBs, we prepared the experimental set-up shown in Figure 3. The reference laser shown in the Figure 3 is turned off for this step. This scheme enables us to measure the frequency up to 20 GHz with ~kHz resolution using a spectrum analyzer. In this set-up, the radiation from both lasers is focused on a schottky diode mixer from VDI (WR 0.4). The horn antenna integrated with the mixer has an accepting aperture with the dimension of 500 μm×500 μm. To achieve a high SNR on the mixer,

two off axid paraboloid mirrors (OAP) are used to focus the beam on to the horn antenna aperture. The DC monitor port of the mixer is connected to a lock-in amplifier to observe light detection by the mixer during optical alignment (indicating the power from π-coupled ADFB). The RF port (related to the product of electric fields if no supermode was formed) is connected to a spectrum analyzer though a 50-dB low noise amplifier.

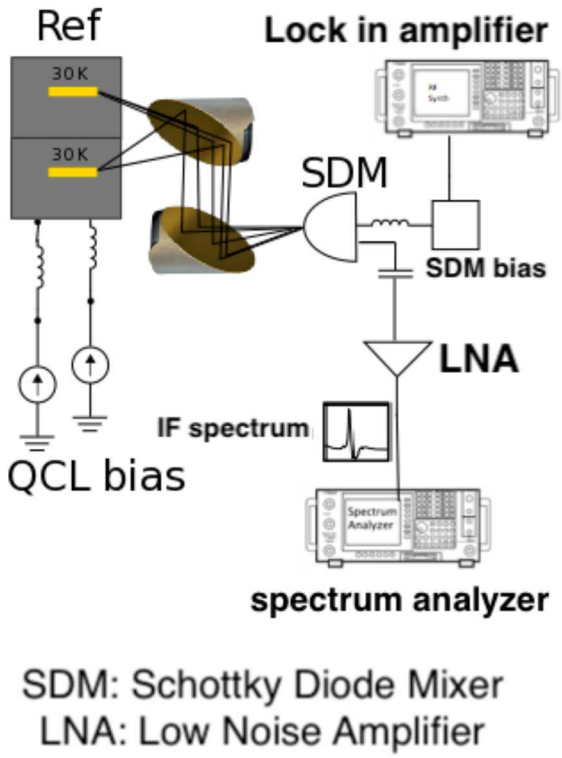

Figure 3: Experimental set-up to measure a possible frequency difference between π-coupled ADFBs.

We have observed single-mode operation (without observing any beat note up to 20 GHz with kHz resolution) in the entire range of bias shown in Figure 2.e This provides strong evidence that the π-coupled scheme is strong enough to maintain a robust phase locking in the entire bias range.

A main motivation for phase-locked ADFBs with separate biases is to achieve frequency tuning using Stark shift in the QCL gain medium. Since changing the relative bias of π-coupled ADFB changes the gain profile, one can deduce from Kramers-Kronig relation[38] that this change

causes changes in the real part of effective index which produce slight frequency shift. Using this Stark shift, π-coupled ADFB can produce continuous frequency tuning with a greater tuning range than a single device as they can act like a master-slave oscillator. Using the same set-up shown in Figure 3, we used a reference π-coupled ADFB on the same die (we did a separate measurement confirming single-mode operation for the reference laser) which was three pairs away from the π-coupled ADFB under investigation. The distant pair is chosen as the reference to ensure a sufficient separation of center frequencies and to avoid a possible local heating. In order to rule out thermal tuning, the lattice temperature for both π-coupled ADFBs were stabilized at 30 K using a Lake Shore PID temperature controller. The frequency of the reference and the π-coupled ADFB measured by FTIR and their relative positions on the die are shown in Figure 4.a. Figure 4.b shows the beat frequency along the current path shown in Figure 4.c (in black line, which was aimed for minimum power variation). Figure 4.d shows the output power of the super mode at corresponding points. We have observed ~10 GHz of frequency tuning with maximum CW output power of ~27 mW. 7 GHz of this frequency change is within 50% power change. Even though we only included a few points in the graph, we observed a complete continuous change on spectral analyzer as we changed the biases along the path provided. No mode hopping was observed. It is worth mentioning that even though 10 GHz is the highest we have achieved in this work, the absolute value of tuning is dependent on the center frequency and active medium type (the more diagonal the transition the greater the Stark shift is) and its dynamic range. In addition, since all off-centered π-coupled ADFB are tested and proved to be single modes, one can design the center frequency of each π-coupled ADFB to be about 10 GHz (for this active medium) apart. In that case, by electrical switching between the π-coupled ADFBs, a much greater continuous tuning range can be achieved.

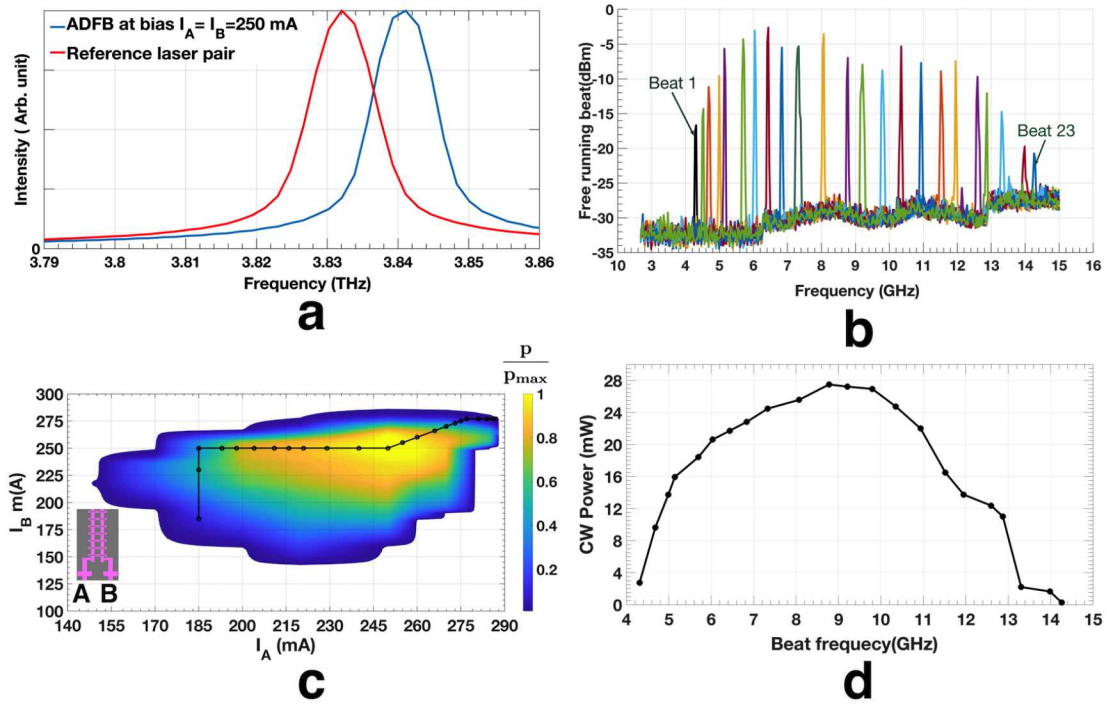

Figure 4: frequency tuning of π-coupled ADFBs, **a**. relative position on the die and the measured frequencies from a FTIR, **b**. frequency difference between the π-coupled ADFB and the reference measured using a schottky diode mixer, **c**. 2-D path for the different bias levels based on the dynamic range and output power consideration, **d**. output power versus the beat frequency.

As it was shown in Fig. 1d, the supermode in π-coupled ADFB has significantly lower mirror loss than the uncoupled counterpart. It is well known that output power from a laser is proportional to $\frac{\alpha_m}{\alpha_m+\alpha_w}$, where α_m is the mirror (radiation) loss and α_w is the waveguide loss[39]. The lasing threshold of the lasers is proportional to $\frac{\alpha_m+\alpha_w}{\Gamma}$ in which Γ is the mode confinement factor. For maximum output without a significant increase of the lasing threshold, $\alpha_m \approx \alpha_w$. In our case, the measured[40] $\alpha_w \sim 15cm^{-1}$. Therefore, one can design individual ADFBs with much higher mirror loss so that the π-coupled ADFB have optimum mirror loss for the symmetric supermode. Here we used another pair of ADFBs and increased the gap size to 6 μm. Simulations suggest a 8 cm^{-1} loss for the symmetric supermode in π-coupled ADFB. The measurement results are shown in Figure 5. Measurement confirms a single-mode frequency at

3.87 GHz with ~ 10 GHz of frequency tuning and ~50 mW of CW power and high-quality beam pattern. The Wall plug efficiency was measured to be 0.71% and the slope efficiency was 263 mW/A. Here, having already proved the continuous nature of frequency shift, we simply measured the spectrum with a FTIR. It should be noted that compared to Fig. 2f, the beam pattern of this device (which is optimized for its output power level) is also more symmetric.

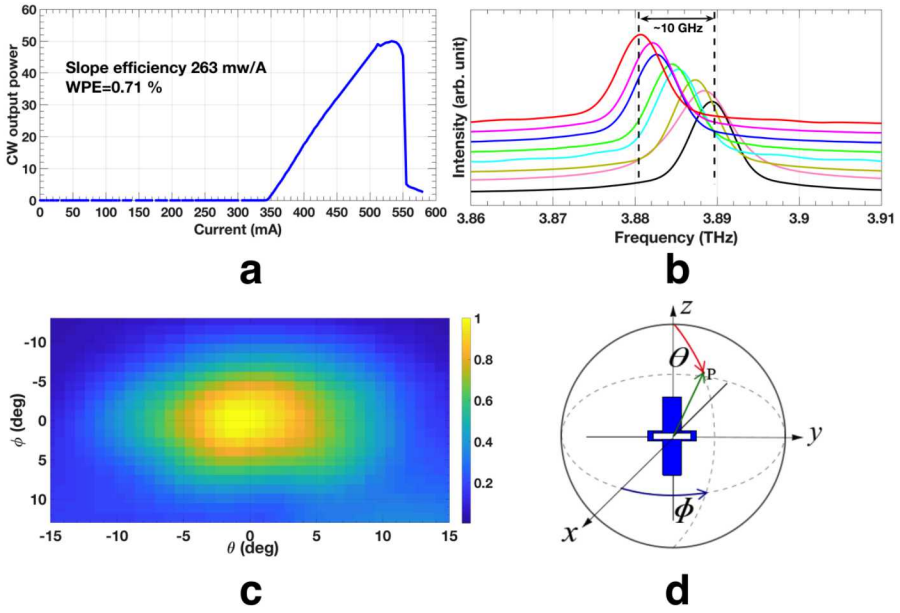

Figure 5: Result of a π-coupled ADFBs optimized for output power, a. I_A=I_B current-light curve, b. spectrum taken by a FTIR on a similar path as fig 4.c, c. beam pattern, and d. illustration of the two angles in the beam-pattern measurement.

In conclusion, we have demonstrated a novel π-coupled scheme to phase lock two ADFBs. The coupling mechanism is strong enough to maintain a robust phase locking at all biases. Tight beam pattern (~ 15^0), ~50 mW of CW power, and ~10-GHz of continuous electrical frequency tuning is demonstrated at 30 K (Temperature performance is discussed in methods section). This platform also promises even higher power levels by phase locking more than two ADFBs, which will also allow for greater frequency tuning than that in a single π-coupled ADFB pair. With the 20-pins connector shown in Fig. 2a (which is by no means the upper limit), one can envision to bias 10 pairs of ADFBs with a frequency separation of ~10 GHz by varying the lengths of the

antenna loops and the periods of the DFB structure. With each pair of ADFB tunable continuously by ~10 GHz, the whole chip can be electrically tuned continuously over ~100 GHz. Such broad and continuous tuning will be highly desirable in sensing and imaging.

[1] Hill, M.T. et al. Lasing in metallic-coated nanocavities. *Nature Photon.* **1**, 589-594 (2007).

[2] Noginov, M.A. et al. Demonstration of a spaser-based nanolaser. *Nature* **460**, 1110-1112 (2009).

[3] Oulton, Rupert F. et al. Plasmon lasers at deep subwavelength scale. *Nature* **461**, 629-632 (2009).

[4] Zhang, J. P. et al. Photonic-Wire Laser. *Phys. Rev. Lett.* **75**, 2678-2681 (1995).

[5] Hill, M. T. & Gather M.C. Advances in small lasers. *Nature Photon.* **8**, 908-918 (2014).

[6] Qin, Qi, et al. "Tuning a terahertz wire laser." Nature photonics3.12 (2009): 732.

[7] Walker, Christopher, et al. "GUSTO: Gal/Xgal U/LDB Spectroscopic-Stratospheric TeraHertz Observatory." American Astronomical Society Meeting Abstracts. Vol. 231. 2018.

[8] Kloosterman, Jenna L., et al. "Hot electron bolometer heterodyne receiver with a 4.7-THz quantum cascade laser as a local oscillator." Applied Physics Letters 102.1 (2013): 011123.

[9] Mirzaei, B., et al. "8-beam local oscillator array at 4.7 THz generated by a phase grating and a quantum cascade laser." Optics express 25.24 (2017): 29587-29596.

[10] Pikel'Ner, S. B. "Structure and dynamics of the interstellar medium." Annual Review of Astronomy and Astrophysics 6.1 (1968): 165-194.

[11] Korter, T. M., and David F. Plusquellic. "Continuous-wave terahertz spectroscopy of biotin: vibrational anharmonicity in the far-infrared." Chemical Physics Letters 385.1-2 (2004): 45-51.

[12] Fitzgerald AJ, Wallace VP, Pye R, et al. Terahertz imaging of breast cancer, a feasibility study. In Infrared and Millimeter Waves, 2004 and 12th International Conference on Terahertz Electronics, 2004. Conference Digest of the 2004 Joint 29th International Conference on. 2004:823–4.

[13] Rahman, Anis, Aunik K. Rahman, and Babar Rao. "Early detection of skin cancer via terahertz spectral profiling and 3D imaging." Biosensors and Bioelectronics 82 (2016): 64-70.

[14] Eadie, Leila H., et al. "Optimizing multi-dimensional terahertz imaging analysis for colon cancer diagnosis." Expert Systems with Applications 40.6 (2013): 2043-2050.

[15] Darmo, Juraj, et al. "Imaging with a Terahertz quantum cascade laser." Optics express 12.9 (2004): 1879-1884.

[16] Bakopoulos, Paraskevas, et al. "A tunable continuous wave (CW) and short-pulse optical source for THz brain imaging applications." Measurement Science and Technology 20.10 (2009): 104001.

[17] Shen Y, Lo T, Taday P, et al. Detection and identification of explosives using terahertz pulsed spectroscopic imaging. Appl Phys Lett. 2005;86:241116.

[18] Duling I, Zimdars D. Terahertz imaging: Revealing hidden defects. Nature Photonics. 2009;3:630–2.

[19] Ogawa, Yuichi, et al. "Interference terahertz label-free imaging for protein detection on a membrane." Optics Express 16.26 (2008): 22083-22089.

[20] Siegel, P. H., and R. J. Dengler. "Applications & early results from THz heterodyne imaging at 119/spl mu/m." Infrared and Millimeter Waves, 2004 and 12th International Conference on Terahertz Electronics, 2004. Conference Digest of the 2004 Joint 29th International Conference on. IEEE.

[21] Khalatpour, Ali, et al. "Unidirectional photonic wire laser." Nature Photonics 11.9 (2017): 555.

[22] Curwen, Christopher A., et al. "Broadband continuous tuning of a THz quantum-cascade VECSEL." CLEO: Science and Innovations. Optical Society of America, 2017.

[23] Xu, Luyao, et al. "Terahertz metasurface quantum-cascade VECSELs: theory and performance." IEEE Journal of Selected Topics in Quantum Electronics 23.6 (2017): 1-12.

[24] Qin, Qi, John L. Reno, and Qing Hu. "MEMS-based tunable terahertz wire-laser over 330 GHz." Optics letters 36.5 (2011): 692-694.

[25] Han, Ningren, et al. "Broadband all-electronically tunable MEMS terahertz quantum cascade lasers." Optics letters39.12 (2014): 3480-3483.

[26] Turčinková, Dana, et al. "Electrically tunable terahertz quantum cascade lasers based on a two-sections interdigitated distributed feedback cavity." Applied Physics Letters 106.13 (2015): 131107.

[27] Ackley, D. E. Single longitudinal mode operation of high power multiple-stripe injection lasers. Appl. Phys. Lett. 42, 152–154 (1983).

[28] Katz, J., Maargalit, S. & Yariv, A. Diffraction coupled phase-locked semiconductor laser array. Appl. Phys. Lett. 42, 554-556 (1983).

[29] Brunner, D. & Fischer, I. Reconfigurable semiconductor laser networks based on diffractive coupling. Opt. Lett. 40, 3854-3857 (2015).

[30] Chen, K.L. & Wang, S. Single-lobe symmetric coupled laser arrays. Electron Lett. 21, 347-349 (1985).

[31] Streifer, W., Welch, D. Cross, P. & Scifres, D. Y-junction semiconductor laser arrays: Part I - Theory. IEEE J. Quantum Electron. 23,744–751 (1987).

[32] Botez, D. & Peterson, G. Modes of phase-locked diode-laser arrays of closely spaced antiguides. Electron. Lett. 24, 1042-1044 (1988).

[33] Botez. D. High-power monolithic phase-locked arrays of antiguided semiconductor diode lasers. Optoelectronics, IEE Proceedings Part J, Optoelectronics, 139, 14–23 (1992).

[34] Kao, T-Y., Hu, Q. & Reno, J.L. Phase-locked arrays of surface-emitting terahertz quantum-cascade lasers. Appl. Phys. Lett. 96, 101106 (2010).

[35] Kao, Tsung-Yu, John L. Reno, and Qing Hu. "Phase-locked laser arrays through global antenna mutual coupling." Nature Photonics 10.8 (2016): 541.

[36] Kao, Tsung-Yu, et al. "Antenna coupled photonic wire lasers." Optics Express 23.13 (2015): 17091-17100.

[37] Amanti, M. I., Fischer, M., Scalari, G., Beck, M. & Faist, J. Low-divergence single-mode terahertz quantum cascade laser. Nat. Photon. 3, 586-590 (2009).

[38] Roessler, D. M. "Kramers-Kronig analysis of reflection data." British Journal of Applied Physics 16.8 (1965): 1119.

[39] Faist, J. Wallplug efficiency of quantum cascade lasers: Critical parameters and fundamental limits. Appl. Phys. Lett. 90, 253512 (2007).

[40] Burghoff, D. et al. A terahertz pulse emitter monolithically integrated with a quantum cascade laser. Appl. Phys. Lett. 98, 061112 (2011).

[41] Chan, Chun Wang I., et al. "Tradeoffs between oscillator strength and lifetime in terahertz quantum cascade lasers." Applied Physics Letters 109.20 (2016): 201104.

METHODS:

Finite element simulations

The simulations were carried out using COMSOL Multiphysics version 5.3. Material loss was not considered and the relative permittivity of GaAs was set to 13. Adhesion layers were not included in the simulations and top and bottom contacts modeled with perfect electric conductor.

Active medium

OWI210H is a three-quantum well GaAs/$Al_{0.15}Ga_{0.85}As$ THz QCL[41]. It has a highly diagonal radiative transition (oscillator strength ~ 0.2) and large injector anticrossing (~1.7-2.0 meV). The doping concentration is 2.6 $x10^{15}$. Pulse mode maximum lasing temperature and emission frequency are ~170K and ~ 3.8 THz . Average doping was verified using secondary ion mass spectroscopy (SIMS) performed by Evans Analytical Group.

L-I-V & Spectrum measurement

For pulsed L–I–V measurements and cw measurements, the lasers were operated at a temperature of 30 K. The relative optical power was measured with a QMC pyroelectric detector and mechanically chopped at 100 Hz. Spectra were measured using a Fourier Transform Infrared Spectrometer (FTIR; model Thermo Nicolet 6700) with internal Deuterated TriGlycine Sulfate (DTGS) detector

Absolute Power measurement

The relative power measured from pyroelectric detector was calibrated using a Thomas Keating absolute terahertz power meter at a 30 Hz mechanical chopping frequency without any focusing

optics between the laser and the power meter except a high-density polyethylene window on the cryostat. The laser under test was operated in cw at a temperature of 30 K inside a Cryomech Pulse tube cryorefrigerator (model PT 810). Maximum lasing temperature was 121 K for pulse and 75 K for cw operations. Power dropped to 50% at 70 K for pulse and 57 K for CW mode.

Beam pattern measurement

Far-field beam patterns are measured with a pyroelectric detector mounted on a two-dimensional motorized scanning stage which is placed at 10 cm from the lasers scanning between ±30◦ for both directions without any optics between the laser and the detector. Laser is operated near the peak power in pulsed mode with 10% duty-cycle and electronically chopped at 100 Hz.

Acknowledgements:

This work is supported by National Aeronautics and Space Administration (NASA) and National Science Foundation (NSF) at MIT. This work was performed, in part, at the Center for Integrated Nanotechnologies, an Office of Science User Facility operated for the U.S. Department of Energy (DOE) Office of Science. Sandia National Laboratories is a multi-program laboratory managed and operated by Sandia Corporation, a wholly owned subsidiary of Lockheed Martin Corporation, for the U.S. Department of Energy's National Nuclear Security Administration under contract DE-AC04-94AL85000.

Contributions:

A.K. conceived the idea, strategy, designed and fabricated the devices and performed the measurements and analysis. J.L.R. provided the material growth. All the work was done under the supervision of Q.H.

Competing Financial Interests:

The authors declare no competing financial interests.

Corresponding author:

Correspondence to Q.H

Data Availability

The data that support the plots within this paper and other findings of this study are available from the corresponding author upon reasonable request.